iScience

Article

Dopaminergic neurons are vulnerable to dysregulation of YEATS2-dependent calcium homeostasis

Graphical abstract

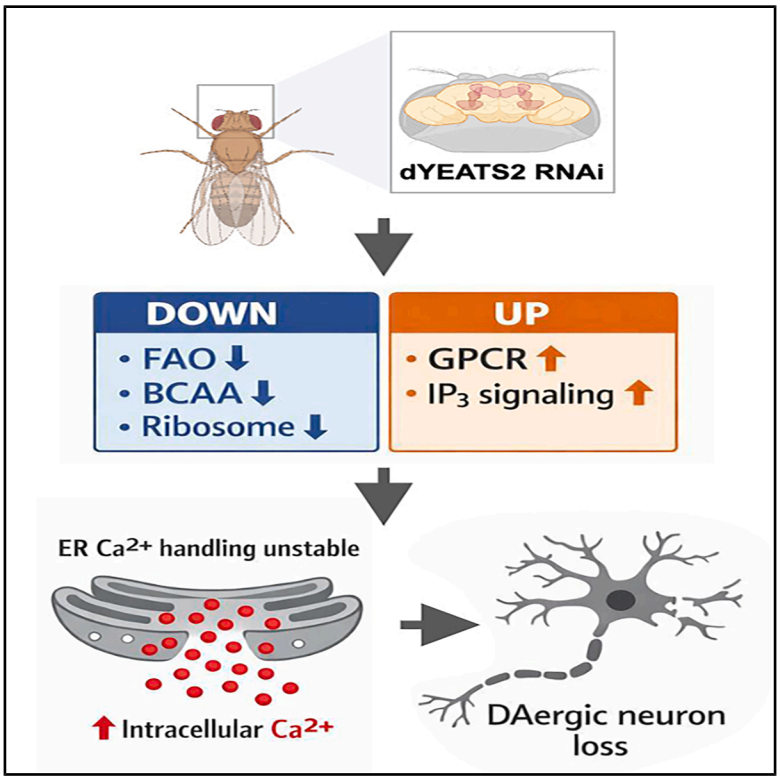

Authors

Luca Lo Piccolo, Ranchana Yeewa, Pitiporn Noisagul, Arnaud Monteil, Vorasuk Shotelersuk, Salinee Jantrapirom

Correspondence

lopiccolo.l@cmu.ac.th (L.L.P.), salinee.jan@cmu.ac.th (S.J.)

In brief

Epigenetics; Molecular neuroscience

Highlights

- YEATS2 knockdown alters neuronal metabolic and GPCR signaling programs
- YEATS2 loss is associated with brain-wide calcium changes and DA neuron stress
- Modulating Orai- and RyR-dependent calcium flux mitigates major phenotypes
- YEATS2 contributes to an epigenetic-calcium axis in dopaminergic neurons

Lo Piccolo et al., 2026, iScience *29*, 115855
June 19, 2026
https://doi.org/10.1016/j.isci.2026.115855

CellPress

iScience

CellPress
OPEN ACCESS

Article

Dopaminergic neurons are vulnerable to dysregulation of YEATS2-dependent calcium homeostasis

Luca Lo Piccolo,[1,8,*] Ranchana Yeewa,[1] Pitiporn Noisagul,[1] Arnaud Monteil,[2,3] Vorasuk Shotelersuk,[4,5] and Salinee Jantrapirom[6,7,*]

[1]Center of Multidisciplinary Technology for Advanced Medicine (CMUTEAM), Faculty of Medicine, Chiang Mai University, Chiang Mai, Thailand
[2]Institut de Génomique Fonctionnelle, Université de Montpellier, CNRS, INSERM, Montpellier, France
[3]Department of Physiology, Faculty of Medicine Siriraj Hospital, Mahidol University, Bangkok, Thailand
[4]Center of Excellence for Medical Genomics, Department of Pediatrics, Faculty of Medicine, Chulalongkorn University, Bangkok, Thailand
[5]Excellence Center for Genomics and Precision Medicine, King Chulalongkorn Memorial Hospital, The Thai Red Cross Society, Bangkok, Thailand
[6]Department of Pharmacology, Faculty of Medicine, Chiang Mai University, Chiang Mai, Thailand
[7]*Drosophila* Centre for Human Diseases and Drug Discovery (DHD), Faculty of Medicine, Chiang Mai University, Chiang Mai, Thailand
[8]Lead contact
*Correspondence: lopiccolo.l@cmu.ac.th (L.L.P.), salinee.jan@cmu.ac.th (S.J.)
https://doi.org/10.1016/j.isci.2026.115855

SUMMARY

YEATS2 is a chromatin-associated factor that regulates dopaminergic (DAergic) synaptic integrity, although its mechanism of action remains unclear. Here, we profiled head transcriptomic changes following neuron-specific *YEATS2* knockdown in *Drosophila*. This analysis revealed coordinated downregulation of metabolic genes alongside upregulation of G protein-coupled receptor (GPCR) signaling components. YEATS2 loss led to elevated intracellular calcium, indicating calcium overload in the nervous system, and was associated with seizure-like activity, locomotor deficits, and loss of DAergic neurons, while sparing glutamatergic neurons and mushroom bodies. Genetic and pharmacological inhibition of store-operated calcium entry (SOCE) via the Orai channel, as well as blockade of ryanodine receptors, improved stress-induced phenotypes, restored calcium balance, and preserved DAergic neuron integrity. Together, these findings identify ER-centered calcium dysregulation as a key downstream consequence of YEATS2 loss and define a YEATS2-dependent epigenetic-calcium axis that links chromatin regulation to neuronal excitability and selective dopaminergic vulnerability.

INTRODUCTION

YEATS2 is a chromatin-associated protein that selectively recognizes histone crotonylation, recruiting chromatin remodeling complexes and transcriptional co-factors to regulate gene expression programs essential for cellular differentiation and homeostasis.[1–3] While extensively studied in cancer, especially solid tumors, YEATS2's roles in non-malignant tissues remain largely unexplored.[4,5] In *Drosophila*, the YEATS2 ortholog (also known as D12 and hereafter named as dYEATS2) retains a highly conserved YEATS domain (45.2% identity)[6] and has been reported as a component of the ATAC complex,[7,8] supporting an evolutionarily conserved chromatin-associated function and providing a suitable *in vivo* model to investigate YEATS2 biology in neurons. Our recent work in *Drosophila* showed that neuron-specific knockdown of *dYEATS2* disrupts dopaminergic (DAergic) synaptic integrity and induces seizure-like behaviors, highlighting YEATS2 as a key regulator of neuronal stability.[9]

DAergic neurons govern motor control, reward processing, and a broad spectrum of cognitive functions, integrating signals across neural circuits underlying voluntary movement, motivation, and learning.[10,11] Despite their importance, these neurons exhibit selective vulnerability in Parkinson's disease (PD), where their progressive loss leads to debilitating symptoms.[12] Multiple stressors, including high metabolic demand, dopamine oxidation, calcium imbalance, mitochondrial dysfunction, and α-synuclein aggregation, have been implicated in this vulnerability. Yet, how these factors coalesce to drive selective DAergic neuron degeneration remains incompletely understood, impeding therapeutic advances.

Epigenetic regulation has emerged as a critical modulator of neuronal identity, plasticity, and survival. Perturbations in epigenetic mechanisms profoundly disrupt DAergic neuron function by triggering maladaptive gene expression and increasing susceptibility to stress.[13] However, the epigenetic factors and downstream pathways that mediate DAergic neuron resilience and vulnerability remain largely undefined.

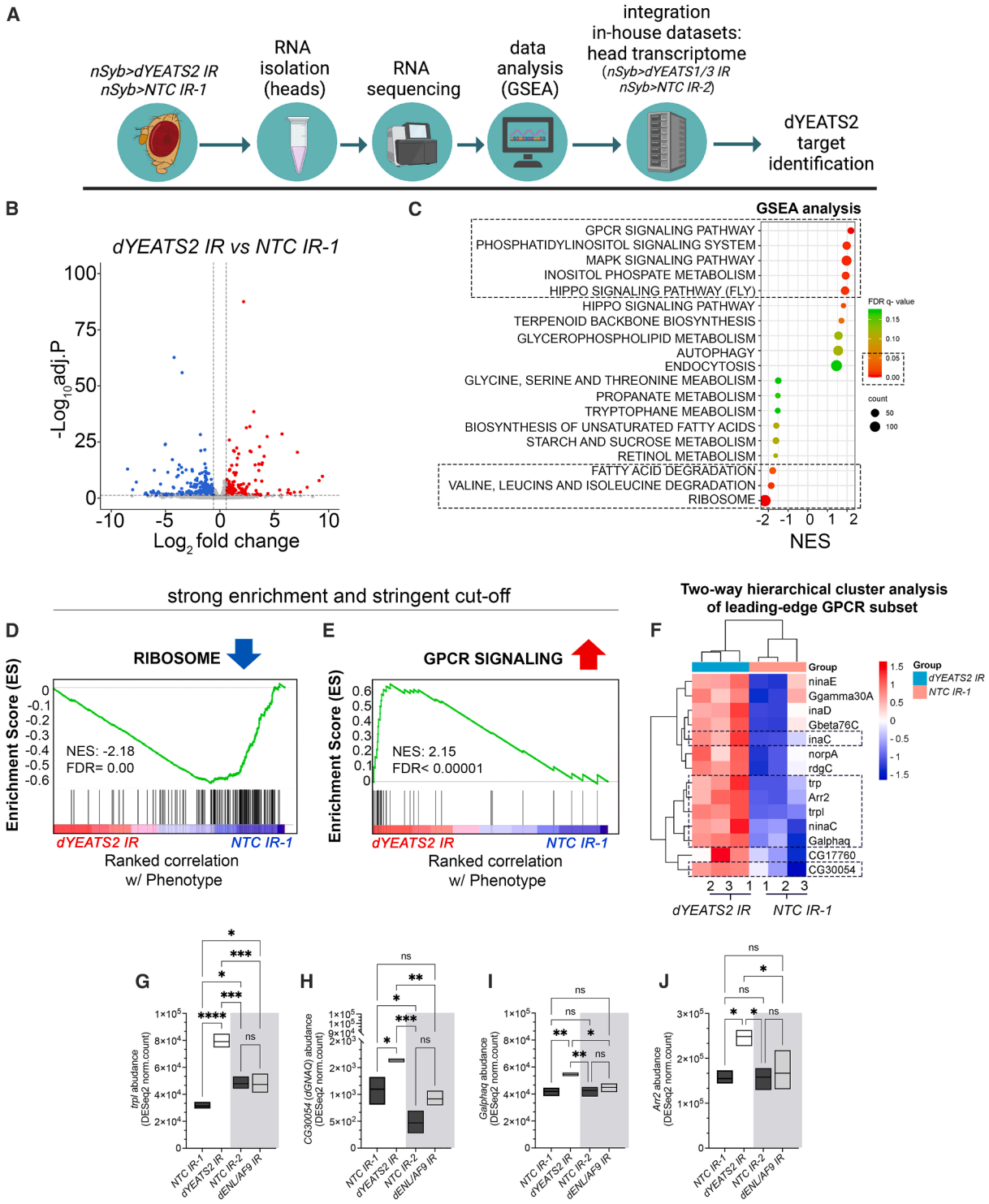

Figure 1. YEATS2 knockdown alters brain transcriptome with enrichment for metabolic and GPCR signaling genes

(A) Schematic of the RNA-seq workflow. Brains with pan-neuronal *dYEATS2* knockdown (*dYEATS2-IR*) were compared to a non-targeting control (*NTC IR-1*), using RNA extracted from 50 brains per replicate across three biological replicates (150 brains per group). To assess target specificity, additional comparisons were made with in-house RNA-seq datasets from *YEATS* paralog knockdowns (*dENL/AF*) and a second independent control (*NTC IR-2*).

(B) Volcano plot shows differentially expressed genes (DEGs) in *dYEATS2-IR* brains, with a total of 1,160 DEGs identified (284 upregulated and 876 down-regulated). Up-regulated genes ($log_2FC > 0.585$, FDR <0.05) are in red; down-regulated genes ($log_2FC < -0.585$, FDR <0.05) in blue; non-significant genes in gray.

(legend continued on next page)

Investigating how YEATS2, as an epigenetic regulator, contributes to DAergic neuron integrity could reveal key molecular mechanisms underlying their selective vulnerability and the networks that safeguard neuronal health. In this study, we address this question by characterizing the transcriptional consequences of neuronal YEATS2 depletion and assessing its impact on DAergic neuron survival.

RESULTS

dYEATS2 knockdown induces transcriptional shifts in neuronal signaling and metabolism

To investigate the molecular consequences of neuronal *YEATS2* depletion, we performed RNA-seq on *Drosophila* heads with pan-neuronal *dYEATS2* knockdown (*dYEATS2-IR*) and compared these to *non-targeting control* (*NTC IR-1*), as well as additional in-house controls, including knockdown of the YEATS paralog *dENL/AF9* and a second *non-targeting control* (*NTC IR-2*) (Figure 1A and Table S1). Raw and DESeq2-normalized RNA-seq data have been deposited in the Gene Expression Omnibus (GSE:GSE307078). We performed gene set enrichment analysis (GSEA) to identify biological pathways significantly affected by YEATS2 depletion (Figures 1B and 1C). To prioritize the most robust and biologically relevant pathways, we applied stringent cutoffs, normalized enrichment score (NES) > 2 and false discovery rate (FDR q) < 0.05 (Figures 1C–1E). This approach enhanced specificity and enabled us to dissect key regulatory networks perturbed by YEATS2 deficiency.

Consistent with prior studies in non-small cell lung cancer models,[14] we observed significant downregulation of genes encoding ribosomal proteins and translation machinery following *YEATS2* knockdown (Figures 1D and S1). This conserved transcriptional signature across species and cell types supports an essential housekeeping role for YEATS2 in sustaining fundamental cellular processes. Given YEATS2's established function as a component of the ATAC chromatin remodeling complex, which promotes gene activation at H3K27ac-enriched promoters, this downregulation likely reflects a direct consequence of disrupted chromatin-mediated gene activation.

Although our stringent cutoffs limited detailed analysis of metabolic genes downregulated by dYEATS2 depletion, such as fatty acid oxidation (FAO) and branched chain amino acid (BCAA) degradation (Figure 1C), it is noteworthy that YEATS family proteins have been implicated in regulating cellular metabolism across diverse organisms.[15–17] This evolutionary conservation, from yeast to humans, underscores their fundamental role in translating metabolic states into transcriptional and epigenetic outputs.

Alongside ribosomal gene downregulation, we detected prominent upregulation of G protein-coupled receptor (GPCR) signaling genes and phosphatidylinositol pathway components. Two-way hierarchical clustering of leading-edge genes revealed distinct grouping patterns among replicates and highlighted major gene expression changes associated with *YEATS2* knockdown (Figures 1F–1J). We focused on *trpL*, *CG30054*, *GalphaQ*, and *Arr2* for further analysis due to their consistent upregulation and known roles in neuronal GPCR signaling and calcium regulation. Specifically, *trpL* encodes a transient receptor potential (TRP)-like channel involved in calcium influx; *CG30054* is predicted to enable G protein-coupled receptor binding activity and to be involved in signal transduction pathways; *GalphaQ* is the guanine nucleotide-binding protein subunit alpha and functions as a G protein alpha subunit mediating GPCR signaling; and *arrestin 2* (*Arr2*) regulates GPCR desensitization and internalization.[18,19] While other genes, such as *inaC* and *nina*C were also upregulated, their functions are more specialized to phototransduction and thus less directly relevant to DAergic neuron signaling.[20] These expression changes were subsequently validated by RT-qPCR (Figure S2). Because YEATS2 does not function as a classical transcriptional repressor, the observed GPCR upregulation likely arises indirectly through compensatory or secondary mechanisms triggered by YEATS2 depletion and associated cellular stress. Mechanistically, this induction may represent an adaptive response to maintain neuronal homeostasis when core transcriptional programs are perturbed. Similarly, increased *trp-L* expression may reflect a compensatory response to metabolic stress, as TRP channels are known to be sensitive to ATP depletion and anoxic conditions.[21] To assess whether the upregulation of TRP-family channels functionally contributes to the stress sensitivity associated with dYEATS2 depletion, we examined recovery time following electric shock at the larval stage, a well-established measure of acute neuronal stress susceptibility in the *Drosophila* nervous system. Because suitable *trpl* RNAi lines were not available in a configuration compatible with genetic interaction studies with *dYEATS2*-RNAi, we employed RNAi against *trp*, a closely related and functionally overlapping TRP-family channel. Using this assay to probe potential functional interaction between *trp* and dYEATS2, we found that the genetic reduction of *trp* in the dYEATS2-RNAi background did not alter recovery time (Figure S3). While this analysis focuses specifically on acute stress sensitivity, a prominent feature of dYEATS2 loss, potential effects on other neuronal or sensory behaviors were not examined in this study.

More broadly, these findings suggest that YEATS2 functions as a hub within complex cellular networks rather than a simple

(C) Gene set enrichment analysis (GSEA) of DEGs. Selected gene sets with FDR q-values <0.15 are shown. Dotted boxes highlight gene sets with FDR q < 0.05 considered for further analysis.

(D and E) GSEA with a stringent cutoff (normalized enrichment score [NES] > 2) identified strong enrichment for ribosome-related genes (down-regulated) and G protein-coupled receptor (GPCR) signaling genes (up-regulated).

(F) Two-way hierarchical clustering of leading-edge genes in the GPCR signaling gene set. Dotted boxes highlight genes with consistent expression patterns across replicates, including *trpL*, *CG30054*, *GalphaQ*, and *Arr2*.

(G–J) Normalized expression counts for selected GPCR genes in control (*dYEATS2-IR*), and additional internal controls (*NTC IR-2* and *dENL/AF9-IR*). Data show increased expression specific to *dYEATS2* knockdown. Data are presented as box-and-whisker plots. Statistical significance was determined using one-way ANOVA with Tukey's multiple comparisons test. $^{*}p < 0.05$, $^{**}p < 0.01$, $^{***}p < 0.001$, and $^{****}p < 0.0001$; ns, not significant.

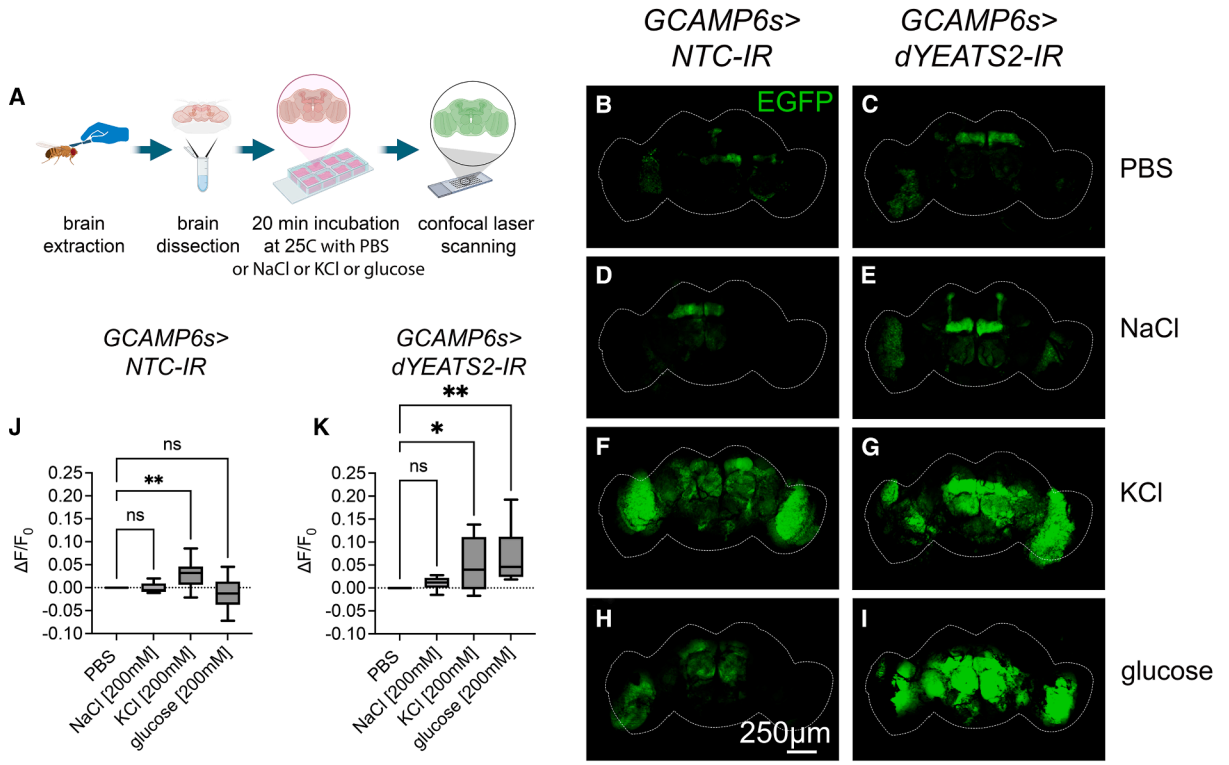

Figure 2. YEATS2 depletion induces calcium overload in adult fly brains, revealed by *ex vivo* GCaMP6s imaging

(A) Schematic of the experimental paradigm. Adult *Drosophila* brains express the genetically encoded calcium indicator GCaMP6s and *dYEATS2* RNAi under pan-neuronal control (*GCaMP6s>dYEATS2-IR*) were dissected and incubated *ex vivo* for 20 min at 25 °C in PBS, 200 mM NaCl, 200 mM KCl, or 200 mM glucose. Brains co-expressing GCaMP6s and a *non-targeting mCherry RNAi* (*GCaMP6s>NTC-IR*) served as controls. For each condition, 10 brains were analyzed per group.

(B–I) Representative confocal images of adult brains acquired in anterior-posterior orientation, presented as maximum intensity projections from 12 optical sections (4 µm each). GCaMP6s fluorescence reflects intracellular calcium levels. Scale bars, 250µm.

(J and K) Quantification of relative calcium signals ($\Delta F/F_0$), normalized to the PBS baseline to account for differences in GCaMP expression across genotypes, following stimulation with NaCl, KCl, or glucose. Data are presented as mean ± SEM. Statistical analyses were performed using one-way ANOVA with Dunnett's post hoc test. $^*p < 0.05$ and $^{**}p < 0.01$; ns, not significant.

molecular switch, illustrating how chromatin regulators integrate epigenetic, metabolic, and signaling cues to preserve neuronal integrity. Notably, both GPCR and phosphatidylinositol signaling pathways converge on intracellular processes that modulate calcium dynamics,[22] suggesting that calcium homeostasis could be disrupted as a downstream consequence. Taken together, these coordinated transcriptional shifts reflect both downregulation of core translational machinery and upregulation of neuronal signaling pathways, highlighting YEATS2's broad impact on gene expression programs controlling metabolism and signal transduction.

dYEATS2 deficiency disrupts calcium homeostasis in adult *Drosophila* brains

Given that intracellular calcium is a common regulatory node for both GPCR and phosphatidylinositol signaling, the transcriptional signature induced by *dYEATS2* depletion implicates calcium homeostasis as a downstream axis connecting chromatin misregulation to neuronal dysfunction. To directly test this hypothesis, we expressed the genetically encoded calcium indicator GCaMP6s[23] pan-neuronally and performed *ex vivo* imaging of adult fly brains. Brains were incubated in PBS, NaCl, KCl, or glucose, and relative calcium responses ($\Delta F/F_0$) were quantified after normalization to the PBS baseline to account for potential differences in GCaMP expression between genotypes (Figure 2A). This whole-brain Ca^{2+} imaging approach provided an initial, unbiased assessment of network-level alterations in neuronal activity caused by dYEATS2 depletion, while future studies using primary neuronal cultures may offer further mechanistic insights into calcium homeostasis at the single-cell level.

Under these conditions, both control and dYEATS2-depleted neurons responded to KCl with increased calcium levels; however, only dYEATS2-depleted neurons exhibited a robust calcium elevation in response to glucose, indicating a genotype-specific hypersensitivity to metabolic stimulation (Figure 2). These results indicate that dYEATS2 deficiency sensitizes neurons to physiological stimuli, reflecting impaired control of intracellular calcium flux. Mechanistically, the enhanced calcium responses are consistent with the transcriptional upregulation of *GalphaQ/IP3* signaling pathway, which is a well-established regulator of calcium entry.[24] By linking *dYEATS2* depletion to exaggerated calcium dynamics, these findings underscore an

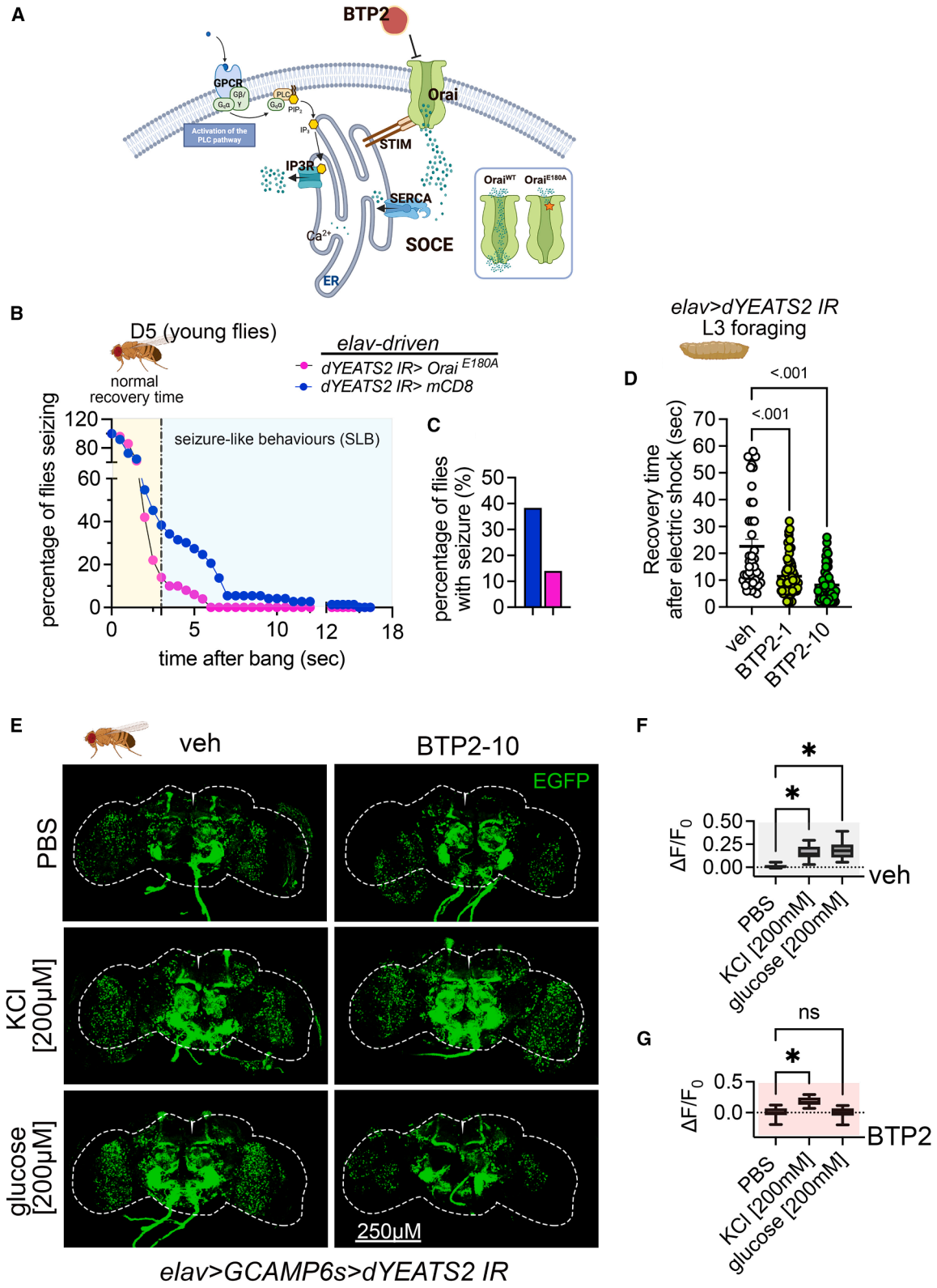

(legend on next page)

epigenetic-to-physiological axis whereby the disruption of chromatin regulation propagates downstream to perturb neuronal homeostasis. This state of neuronal hypersensitivity likely predisposes neurons to functional stress and hyperexcitability, offering a mechanistic explanation for the seizure-like behaviors previously observed in dYEATS2-deficient flies.[9]

To assess causality, we attempted to mitigate these calcium abnormalities. Initial targeting of Gαq, a GPCR effector upregulated upon *dYEATS2* knockdown, was lethal when co-expressed with *dYEATS2 RNAi*, highlighting the essentiality of precise GPCR signaling in neuronal viability. As an alternative, we modulated store-operated calcium entry (SOCE) via the Orai channel (Figure 3A), a key mediator of calcium influx in neurons.[25] Interestingly, pan-neuronal expression of a dominant-negative Orai^{E180A}[26] significantly reduced seizure-like behaviors in adults (Figure 3B), while pharmacological inhibition using the pyrazole derivative BTP2[27] improved recovery times following electric stimulation in larvae expressing *dYEATS2-IR* pan-neuronally (Figure 3C). Consistent with these behavioral improvements, BTP2 administration also attenuated the heightened intracellular Ca^{2+} response to metabolic stimulation in dYEATS2-deficient brains, indicating effective normalization of pathological calcium signaling (Figures 3E–3G). Although Orai^{E180A} expression can affect flight-related locomotion behavior in *Drosophila*,[28] the bang assay specifically measures seizure-like activity and recovery following mechanical stress. Therefore, the suppression of seizure-like phenotypes observed in dYEATS2-depleted flies by either Orai^{E180A} expression or pharmacological inhibition with BTP2 more likely reflects a functional interaction with dYEATS2-dependent pathways, rather than a nonspecific effect on motor performance.

Current genetic constraints preclude testing wild-type Orai overexpression in the dYEATS2-RNAi background; future approaches that enhance Orai/SOCE activity will be important to further delineate the contribution of SOCE to intracellular calcium elevation in dYEATS2-deficient neurons.

To examine whether the observed rescue was specific to the modulation of SOCE or could also be achieved by targeting other calcium pathways, we pharmacologically manipulated additional calcium channels implicated in neuronal calcium homeostasis (Figure S4A). Modulation of voltage-gated calcium channels (VGCCs) using gabapentin, which reduces calcium influx via the evolutionary conserved α2δ subunit in *Drosophila*,[29,30] did not improve recovery time following electric shock in larvae expressing dYEATS2 RNAi pan-neuronally (Figure S4B). In contrast, inhibition of ryanodine receptors (RyRs), intracellular calcium-release channels found on the endoplasmic reticulum of all cells,[31] using dantrolene[32] was associated with a significant improvement in seizure recovery (Figure S4C). Although these observations do not establish a definitive mechanism, they are consistent with a contribution of intracellular calcium store dysregulation, rather than VGCC-mediated calcium influx, to the neuronal phenotypes observed upon dYEATS2 depletion. In combination with the transcriptomic changes in calcium- and inositol-signaling pathways, these findings suggest that YEATS2 loss may influence ER-associated calcium homeostasis, contributing to neuronal vulnerability and increased excitability.

Calcium overload resulting from *dYEATS2* knockdown drives DAergic neuron loss

Given that the depletion of dYEATS2 in the nervous system reduces tyrosine hydroxylase (TH) expression and dopamine levels[9] and having established that dYEATS2 deficiency elevates intracellular calcium and sensitizes neurons to physiological stimuli, we next asked whether this calcium perturbation compromises the integrity of DAergic neurons. To test this, we generated a stable fly line co-expressing *mCD8::EGFP* and *dYEATS2 RNAi* under pan-neuronal control, confirming proper GFP labeling and expected reductions in both *dYEATS2* and TH (Figure S5).

Analysis of DAergic neuron clusters in young adult flies revealed a pronounced loss of neurons, whereas other populations were largely preserved (Figures 4A, 4B, 4G, and S6). Glutamatergic neurons, which constitute most excitatory neurons in the fly brain, displayed normal cluster numbers (Figures 4C, 4D, and 4H), and mushroom body architecture, representing higher-order associative circuits, was unaltered (Figures 4E and 4F).

Figure 3. Inhibition of store-operated calcium entry (SOCE) via Orai channel ameliorates YEATS2 neurological dysfunctions

(A) Schematic model illustrating the role of Orai-mediated SOCE in GPCR-induced calcium dynamics. GPCR activation promotes intracellular calcium release from the endoplasmic reticulum (ER), followed by calcium re-entry through the Orai channel. To genetically inhibit SOCE, a dominant-negative form of Orai (*Orai^{E180A}*) was expressed pan-neuronally in the *dYEATS2* RNAi background. Pharmacological inhibition was achieved by feeding adult flies with BTP2 (YM-58483), a selective Orai channel antagonist.

(B and C) Suppression of seizure-like behavior (SLB) by targeting Orai in adult flies. Adult flies expressing a pan-neuronal dominant-negative Orai mutant (*Orai^{E180A}*) in a *dYEATS2* knockdown background were assessed for SLB. Control flies were age- and sex-matched and expressed *dYEATS2* RNAi in an mCD8 background. SLB was assessed at 5 days post-eclosion following mechanical stimulation (“bang” assay). Flies that recovered within 3 s were classified as normal; longer recovery indicated SLB. The percentage of flies exhibiting SLB was significantly reduced by the genetic or pharmacological inhibition of Orai (n = 45 flies per group).

(D) Pharmacological inhibition of Orai with BTP2 reduces delayed recovery after electric shock in third-instar larvae expressing *dYEATS2* RNAi pan neuronally. Larvae were treated with either 1 μM or 10 μM BTP2 or vehicle control, and time to recovery was measured (n = 75 larvae per group). Individual data points are shown. Statistical significance was assessed using one-way ANOVA followed by Šidák’s post hoc testing; differences with $p < 0.05$ were considered statistically significant.

(E) Representative anterior-posterior confocal projections of adult brains generated from 12 optical slices (4 μm each) are shown. Flies express GCaMP6s in a pan-neuronal dYEATS2 knockdown background and were either treated with 10 μM BTP2 or left untreated (vehicle, veh). GCaMP6s fluorescence serves as a readout of intracellular calcium. Scale bars, 250μm.

(F and G) Quantification of relative calcium signals ($\Delta F/F_0$), normalized to the PBS baseline to account for differences in GCaMP expression across genotypes, following depolarizing (KCl) and metabolic (glucose) stimulation. Data are presented as mean ± SEM. Statistical analyses were performed using one-way ANOVA with Dunnett’s post hoc test. *$p < 0.05$; ns, not significant.

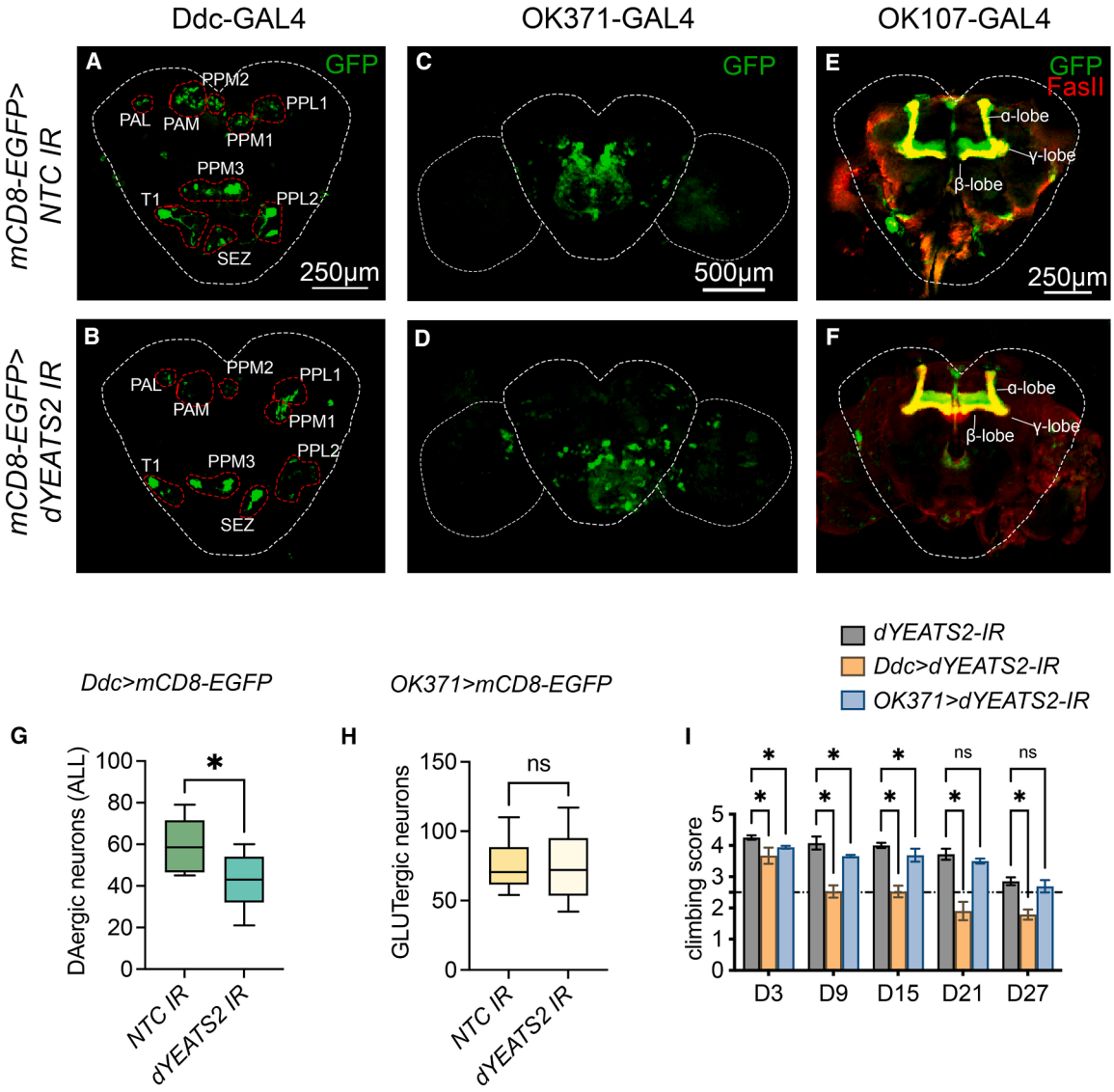

Figure 4. Calcium overload resulting from *dYEATS2* knockdown drives DAergic neuron loss

(A–F) Representative confocal images of distinct neuronal populations in adult *Drosophila* brains expressing membrane-bound mCD8-EGFP, driven by cell-type-specific GAL4 lines, in the presence of *dYEATS2* RNAi (*mCD8-EGFP* > *dYEATS2*-IR) or a non-targeting RNAi control (*mCD8-EGFP* > *NTC-IR*).

(A and B) Dopaminergic neurons were visualized using Ddc-GAL4. Brains are shown in posterior-to-anterior orientation; central brain regions are outlined (dotted lines), and major dopaminergic clusters, including PAL, PAM, PPL1, and PPM3, are circled in red. Scale bars, 250µm.

(C and D) Glutamatergic neurons were labeled using *OK371-GAL4*. The central brain and optic lobes are demarcated by dotted outlines. Scale bars, 500µm.

(E and F) Mushroom body neurons were visualized by FasII staining in brains expressing EGFP under *OK107-GAL4* control; α, β, and γ lobes are indicated. Scale bars, 250µm.

(G) Quantification of total dopaminergic neurons (n = 10). Additional representative brain images are provided in Figure S4.

(H) Quantification of glutamatergic neurons (n = 10).

(I) Age-dependent locomotor decline assessed via climbing assays in flies expressing *dYEATS2* RNAi under *Ddc-GAL4* (DAergic neurons) or *OK371-GAL4* (GLUTergic neurons) compared with genetic controls *dYEATS2 RNAi* carrying fly line lacking a GAL4 driver (non-driven control, NDC). Behavioral deficits were monitored across multiple timepoints post-eclosion (3, 9, 15, 21, and 27 days). Data represent mean ± SEM. Statistical analyses were performed using one-way ANOVA followed by Dunnett's post hoc tests; *$p < 0.05$; ns, not significant.

These observations indicate a selective vulnerability of DAergic neurons to *dYEATS2* decline, suggesting that calcium dysregulation preferentially destabilizes this population.

This selective susceptibility aligns with established principles that DAergic neurons are uniquely burdened by autonomous peacemaking activity, which engages L-type Ca^{2+} channels and drives sustained calcium influx, imposing extraordinary demands on calcium buffering systems.[33] In this context, *dYEATS2* depletion likely exacerbates chronic calcium elevation beyond neuronal buffering capacity, triggering excitotoxic stress,

metabolic imbalance, and ultimately degeneration. This selective vulnerability may also have network-level consequences, given the established role of dopamine in seizure modulation: D1 receptor signaling promotes excitability, whereas D2 receptor pathways are protective.[34] Accordingly, loss of DA neurons and diminished D2 signaling in dYEATS2-depleted flies could plausibly shift the balance toward hyperexcitability and reduced seizure threshold.

Interestingly, while glutamatergic neuron morphology was unaffected by *dYEATS2* knockdown, behavioral assays revealed reduced locomotor function when *dYEATS2* was depleted specifically under the glutamatergic OK371-GAL4 driver (Figure 4I). The magnitude of impairment was milder than that observed with DAergic-specific knockdown and most prominent in young flies, suggesting that glutamatergic neurons may be functionally sensitive to dYEATS2 deficiency without overt structural degeneration.

These findings reinforce the notion that not all neuronal populations respond equally to transcriptional perturbations of dYEATS2; rather, vulnerability is shaped by intrinsic physiological demands and calcium-buffering capacity, manifesting as distinct degrees of cytotoxicity across cell types.

Given that the downregulation of metabolic genes was also observed in the head transcriptome of *dYEATS2* knockdown flies (Figure S7), impaired energy metabolism likely represents an additional source of neuronal dysfunction. For instance, glutamatergic neurons, which appear morphologically resilient to calcium overload, could still be vulnerable to metabolic insufficiency due to their high energetic demands for sustained synaptic activity.[35] Thus, while DAergic neurons could primarily succumb to calcium-driven excitotoxic stress, glutamatergic populations may experience dysfunction through a distinct, metabolism-based mechanism. These complementary vulnerabilities underscore the multifaceted consequences of dYEATS2 deficiency and illustrate how epigenetic perturbation can differentially compromise neuronal subtypes depending on their physiological and metabolic requirements. Although our observations suggest selective vulnerability of DAergic neuron clusters, direct transcriptional profiling of these versus resistant neurons was not performed. Future studies examining gene expression in distinct neuronal populations will be important to confirm the cell-type specificity of YEATS2's effects on chromatin and transcription.

Targeting SOCE and RyR confirms calcium-dependent vulnerability of DAergic neurons in *dYEATS2*-deficient flies

Given that *dYEATS2* depletion leads to elevated intracellular calcium and correlates with DAergic neuron loss, we investigated whether calcium overload directly drives this selective neurodegeneration. To test this, we pharmacologically attenuated SOCE using the Orai inhibitor BTP2, previously shown to improve neurobehavioral deficits in *dYEATS2*-deficient flies. We then assessed DAergic neuron structural integrity in adult flies expressing *mCD8-GFP* and *dYEATS2 RNAi* specifically in DA neurons (*Ddc>mCD8-GFP>dYEATS2 IR*; Figure 5A).

Confocal analysis revealed that BTP2 treatment at 1 μM and 10 μM significantly increased the number of TH-positive DA neurons, measured by co-localization of mCD8-GFP and TH immunoreactivity (Figures 5B, 5C, and S8). These results indicate that inhibiting Orai-mediated calcium influx mitigates the structural deficits caused by *dYEATS2* knockdown, establishing maladaptive calcium signaling as a dYEATS2-dependent causal factor in DAergic neuron degeneration.

BTP2 treatment not only increased DAergic neuron numbers but also normalized the expression of calcium signaling genes, including *GαQ* and *trpL*, which are elevated in dYEATS2-deficient neurons (Figure 5D). In parallel, BTP2 restored the expression of *vMAT* and *DD2R*, which were significantly reduced in *dYEATS2*-knockdown flies prior to treatment[9] (Figure 5D). Because expression of these genes is associated with DAergic neuron integrity, their normalization is consistent with a broader restoration of DAergic neuronal health following Orai inhibition. To determine whether limiting calcium release from intracellular stores exerts a similar protective effect, we next examined the impact of the RyR inhibitor dantrolene. Administration of dantrolene (10 μM) significantly increased the number of TH-positive DAergic neurons in dYEATS2-knockdown brains (Figure S9), phenocopying the structural rescue observed following pharmacological inhibition of SOCE with BTP2.

Taken together, the ability of both SOCE inhibition and RyR blockade to ameliorate stress-induced phenotypes supports a model in which ER-centered calcium dysregulation represents a key downstream consequence of YEATS2 loss.

Beyond the acute calcium dysregulation elicited by dYEATS2 depletion, our results suggest that perturbations in crotonate metabolism may also influence calcium signaling in dopaminergic neurons. Because YEATS2 acts as a selective reader of histone crotonylation, its loss may mimic the functional consequences of diminished crotonylation by disrupting the recognition of this chromatin modification. Accordingly, alterations in crotonyl-CoA abundance or in the enzymatic machinery that regulates histone crotonylation could similarly compromise calcium homeostasis, even in the absence of direct genetic mutations. Together, these observations suggest a mechanism whereby metabolic-epigenetic crosstalk converges on calcium signaling to shape dopaminergic neuron vulnerability, offering a conceptual framework for future studies aimed at dissecting selective neuronal susceptibility and identifying potential therapeutic avenues in neurodegenerative disease.

DISCUSSION

This study identifies dYEATS2 as a critical determinant of neuronal calcium homeostasis and DAergic neuron resilience. Neuron-specific depletion of dYEATS2 in *Drosophila* induces a coordinated transcriptional program marked by the downregulation of metabolic pathways, including FAO, BCAA catabolism, and ribosome biogenesis, alongside upregulation of GPCR, inositol, and calcium signaling components. Functionally, these changes are associated with elevated intracellular calcium, loss of DAergic neurons, and heightened sensitivity to acute stress.

Using complementary genetic and pharmacological interventions, we show that inhibiting SOCE through the Orai channel restores intracellular calcium levels, improves stress resilience, and preserves DAergic neuron number and molecular identity.

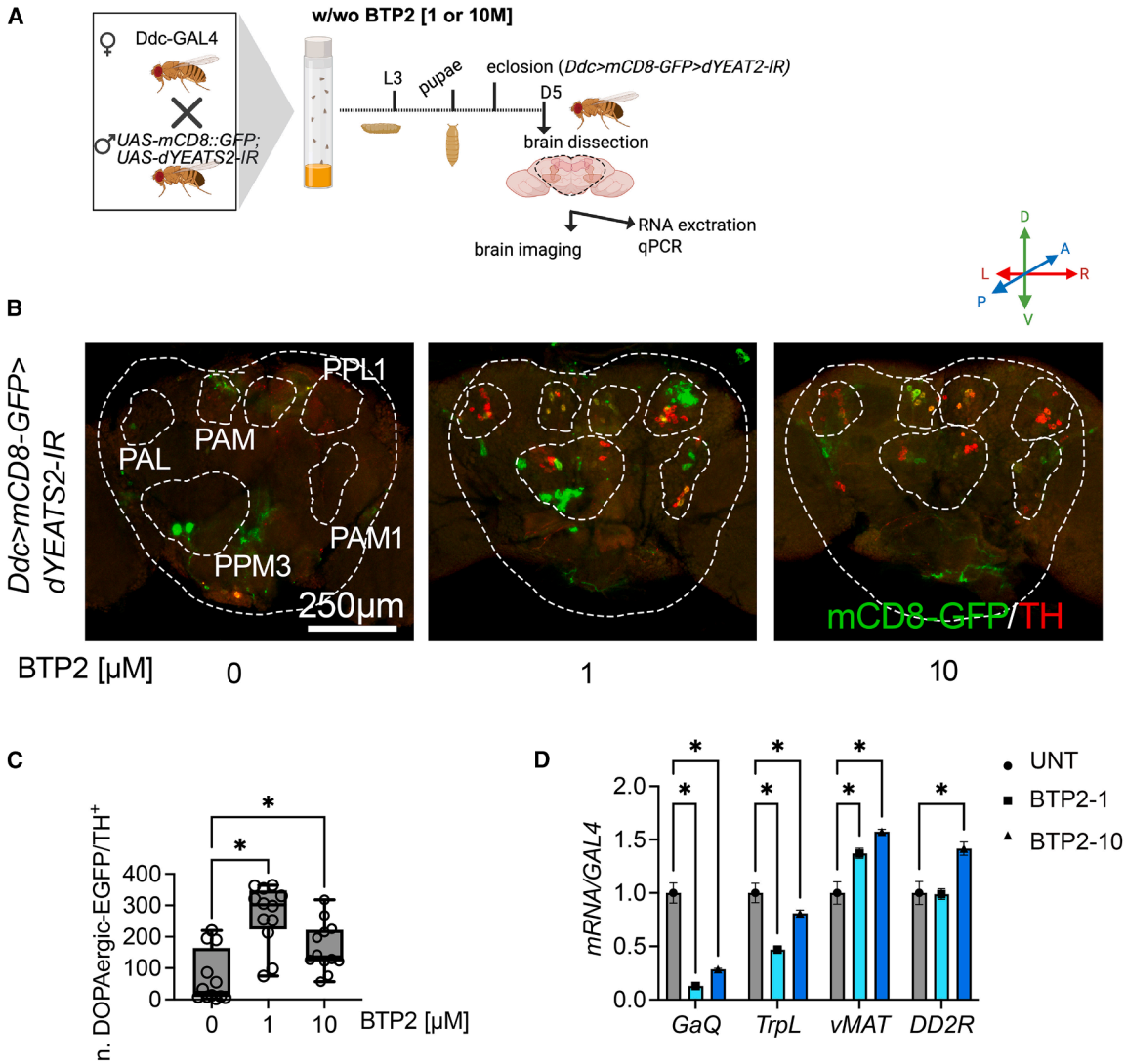

Figure 5. Pharmacological attenuation of SOCE restores DAergic synaptic integrity in *dYEATS2*-deficient flies

(A) Experimental scheme. Flies expressing membrane-tethered mCD8-GFP and *dYEATS2* RNAi specifically in dopaminergic neurons (*Ddc>mCD8-GFP>dYEATS2-IR*) were reared on standard medium supplemented with vehicle or the Orai inhibitor BTP2 (YM-58483) at 1 µM or 10 µM. Adult flies were transferred to fresh vials containing the same treatments, and heads were dissected at 5 days post-eclosion for confocal imaging or RNA extraction.

(B) Representative confocal images (posterior→anterior orientation) showing functionally active DAergic neurons identified by co-localization of mCD8-GFP (membrane marker expressed under Ddc-GAL4 driver) and tyrosine hydroxylase (TH) immunoreactivity. Central brain boundaries are indicated by dotted lines; major DA clusters (PAL, PAM, PPL1, PPM3) are highlighted with red dashed circles. Scale bars, 250µm.

(C) Quantification of EGFP-TH co-localization (number of co-localized puncta) was performed on 10 independent brains per condition using the colocalization module in CellSense (Olympus). Bars show mean ± SEM; BTP2 treatment at both 1 µM and 10 µM significantly increased the number of EGFP-TH co-localizing spots relative to untreated *dYEATS2*-IR animals.

(D) Transcript levels of selected *dYEATS2*-responsive genes (*Gαq*, *trpL*, *vMAT*, and *DD2R*) were measured from dissected adult heads following vehicle or BTP2 treatment to assess whether SOCE inhibition modulates these transcriptional changes. Gene expression was determined by reverse transcription quantitative PCR (RT-qPCR). Data are presented as mean ± SEM. Statistical significance was assessed by one-way ANOVA with Šidák's and Tukey's post hoc tests, respectively; $p < 0.05$ was considered significant.

Likewise, suppressing endoplasmic reticulum calcium release via RyR inhibition with dantrolene produces comparable protective effects. In contrast, blocking VGCCs does not rescue the phenotypes, arguing against plasma membrane depolarization-driven calcium influx as the primary cause. Together, these results point to endoplasmic reticulum-centered calcium dysregulation, involving both calcium entry and release pathways, as a principal contributor to pathological calcium elevation in the context of dYEATS2 loss.

The upstream origin of this ER calcium dysregulation remains unresolved. One plausible model is that impaired neuronal metabolism, arising from reduced FAO and/or BCAA degradation and

translational capacity, compromises ER homeostasis and calcium handling. Consistent with this possibility, studies in other systems have shown that metabolic insufficiency, translational stress, and redox imbalance can disrupt ER function and Ca^{2+} homeostasis, promoting aberrant calcium signaling, particularly in neurons.[36,37] In the dYEATS2-depleted brain, the combined downregulation of mitochondrial and catabolic pathways with reduced ribosome- and translation-related gene expression could therefore sensitize the endoplasmic reticulum to stress and lower the threshold for calcium overload. Alternatively, the transcriptional upregulation of GPCR and inositol signaling components may reflect compensatory remodeling of signaling networks that secondarily enhance calcium mobilization. Discriminating among these possibilities will require defining the direct chromatin targets of dYEATS2 in neurons and testing how specific metabolic and signaling nodes contribute to calcium dysregulation and dopaminergic neuron loss.

Together, these findings support a model in which loss of dYEATS2 alters neuronal gene expression programs in ways that promote endoplasmic reticulum-associated calcium mishandling, leading to calcium overload, hyperexcitability, and selective DAergic vulnerability. By identifying SOCE and RyR-dependent calcium release as modifiable downstream contributors to the phenotypes, this work highlights neuronal calcium homeostasis as a tractable intervention point when chromatin-linked metabolic and stress-response programs are disrupted. More broadly, the dYEATS2-dependent epigenetic-calcium axis defined here provides a framework for understanding how chromatin regulation can shape neuronal excitability and cell-type-selective susceptibility under stress, with potential relevance to neurodegenerative contexts in which epigenetic and metabolic dysfunction converge.

Limitations of the study

Several limitations should be noted. First, while transcriptional changes in GPCR and inositol signaling pathways are robust, it remains unclear whether these alterations reflect direct chromatin regulation by YEATS2 or secondary, compensatory responses to neuronal stress. Second, our functional analyses focus primarily on dopaminergic neurons and acute stress paradigms, leaving open the possibility that additional neuronal subtypes or behaviors are affected through distinct mechanisms. Given that several dysregulated GPCRs are also involved in sensory pathways, particularly odor sensation, future studies employing sensory neuron-specific manipulations and behavioral assays will be important to determine whether GPCR dysregulation has functional consequences beyond calcium homeostasis.

Finally, while our data support calcium dysregulation as a key downstream contributor to neuronal dysfunction, how YEATS2-dependent transcriptional changes give rise to GPCR dysregulation and Orai-mediated calcium overload remains to be determined.

RESOURCE AVAILABILITY

Lead contact

Requests for further information and resources should be directed to and will be fulfilled by the lead contact, Luca Lo Piccolo (lopiccolo.l@cmu.ac.th).

Materials availability

All unique/stable reagents generated in this study are available from the lead contact with a completed materials transfer agreement.

Data and code availability

- RNA-seq data have been deposited in GEO under accession number GSE:GSE307078, and the associated BioProject has been deposited under accession number PRJNA1314219. These data are publicly available as of the date of publication.
- Original western blot images are included in the supplemental information. Microscopy data reported in this paper will be shared by the lead contact upon request.
- This paper does not report original code.
- Any additional information required to reanalyze the data reported in this paper is available from the lead contact upon request.

ACKNOWLEDGMENTS

This work was supported by the Mid-Career Research grant (N42A670768) from the National Research Council of Thailand, Genomics Thailand through the Health Systems Research Institute (HSRI; grant 68-060), the Fundamental Fund of Chiang Mai University (grant FF68/207569), and the Faculty of Medicine, Chiang Mai University (grant FACMED 139/2567). Additional institutional support was provided by Chiang Mai University. We are grateful to Mr. Papon Hitmool, Mr. Sakorn Phongchankhiao, and Mr. Tawan Munwanna (Department of Pharmacology, Faculty of Medicine, Chiang Mai University), as well as Ms. Chansunee Panto (CMUTEAM, Faculty of Medicine, Chiang Mai University), for their invaluable technical and administrative assistance. We also thank the Bloomington Drosophila Stock Center for providing fly strains, and Science and Educational Company Limited (SCIED) for confocal scanning electron microscopy training. We also acknowledge the Robotics Engineering and Artificial Intelligence (REAI), Chiang Mai University, for their technical assistance in improving and maintaining the *Drosophila* Larval Electric Stimulator (DL-ES). We are particularly grateful to Dr. Nithi Asavapanumas (Faculty of Medicine Ramathibodi Hospital, Mahidol University, Thailand) for insightful discussions that inspired us to investigate dantrolene as a ryanodine receptor inhibitor in our experimental model.

AUTHOR CONTRIBUTIONS

Conceptualization: L.LP. and S.J.; data curation: L.LP. and S.J.; formal analysis: L.LP., R.Y., P.N., and S.J.; funding acquisition; L.LP.; investigation: L.LP., R.Y., P.N., and S.J.; methodology: L.LP., R.Y., and P.N.; project administration: L.LP.; resources; L.LP. and S.J.; software: L.LP. and R.Y.; supervision; L.LP.; validation: L.LP. and S.J.; visualization: L.LP., R.Y., and S.J.; writing – original draft: L.LP.; writing – review and editing: All authors have reviewed and approved the final version of this manuscript.

DECLARATION OF INTERESTS

The authors declare no competing interests.

DECLARATION OF GENERATIVE AI AND AI-ASSISTED TECHNOLOGIES IN THE WRITING PROCESS

During the preparation of this work, the author(s) used NotebookLM to generate the graphical abstract and GPT-5.2 to improve the clarity and readability of the discussion section. After using these tools, the author(s) reviewed and edited the content as needed and take full responsibility for the content of the publication.

STAR★METHODS

Detailed methods are provided in the online version of this paper and include the following:

- KEY RESOURCES TABLE

SUPPLEMENTAL INFORMATION

Supplemental information can be found online at https://doi.org/10.1016/j.isci.2026.115855.

Received: September 13, 2025
Revised: February 4, 2026
Accepted: April 20, 2026
Published: April 22, 2026

REFERENCES

1. Orpinell, M., Fournier, M., Riss, A., Nagy, Z., Krebs, A.R., Frontini, M., and Tora, L. (2010). The ATAC acetyl transferase complex controls mitotic progression by targeting non-histone substrates. EMBO J. *29*, 2381–2394. https://doi.org/10.1038/emboj.2010.125.
2. Suganuma, T., Mushegian, A., Swanson, S.K., Abmayr, S.M., Florens, L., Washburn, M.P., and Workman, J.L. (2010). The ATAC acetyltransferase complex coordinates MAP kinases to regulate JNK target genes. Cell *142*, 726–736. https://doi.org/10.1016/j.cell.2010.07.045.
3. Zhao, D., Guan, H., Zhao, S., Mi, W., Wen, H., Li, Y., Zhao, Y., Allis, C.D., Shi, X., and Li, H. (2016). YEATS2 is a selective histone crotonylation reader. Cell Res. *26*, 629–632. https://doi.org/10.1038/cr.2016.49.
4. Roy, J., Kumar, A., Chakravarty, S., Biswas, N.K., Goswami, S., and Mazumder, A. (2025). Dynamic interaction of MYC enhancer RNA with YEATS2 protein regulates MYC gene transcription in pancreatic cancer. EMBO Rep. *26*, 2519–2544. https://doi.org/10.1038/s44319-025-00446-0.
5. Zhai, Y., Zhang, F., Shi, X., Zou, S., Hu, X., Shan, C., Zhang, L., Zou, B., Yang, X., Kong, P., and Cheng, X. (2025). YEATS2 promotes malignant phenotypes of esophageal squamous cell carcinoma via H3K27ac activated-IL6ST. Front. Cell Dev. Biol. *13*, 1497290. https://doi.org/10.3389/fcell.2025.1497290.
6. Yeewa, R., Chaiya, P., Jantrapirom, S., Shotelersuk, V., and Lo Piccolo, L. (2022). Multifaceted roles of YEATS domain-containing proteins and novel links to neurological diseases. Cell. Mol. Life Sci. *79*, 183. https://doi.org/10.1007/s00018-022-04218-0.
7. Suganuma, T., Gutiérrez, J.L., Li, B., Florens, L., Swanson, S.K., Washburn, M.P., Abmayr, S.M., and Workman, J.L. (2008). ATAC is a double histone acetyltransferase complex that stimulates nucleosome sliding. Nat. Struct. Mol. Biol. *15*, 364–372. https://doi.org/10.1038/nsmb.1397.
8. Guelman, S., Suganuma, T., Florens, L., Swanson, S.K., Kiesecker, C.L., Kusch, T., Anderson, S., Yates, J.R., 3rd, Washburn, M.P., Abmayr, S.M., and Workman, J.L. (2006). Host cell factor and an uncharacterized SANT domain protein are stable components of ATAC, a novel dAda2A/dGcn5-containing histone acetyltransferase complex in Drosophila. Mol. Cell Biol. *26*, 871–882. https://doi.org/10.1128/MCB.26.3.871-882.2006.
9. Lo Piccolo, L., Yeewa, R., Pohsa, S., Yamsri, T., Calovi, D., Phetcharaburanin, J., Suksawat, M., Kulthawatsiri, T., Shotelersuk, V., and Jantrapirom, S. (2024). FAME4-associating YEATS2 knockdown impairs dopaminergic synaptic integrity and leads to seizure-like behaviours in Drosophila melanogaster. Prog. Neurobiol. *233*, 102558. https://doi.org/10.1016/j.pneurobio.2023.102558.
10. Ott, T., Stein, A.M., and Nieder, A. (2023). Dopamine receptor activation regulates reward expectancy signals during cognitive control in primate prefrontal neurons. Nat. Commun. *14*, 7537. https://doi.org/10.1038/s41467-023-43271-6.
11. Puig, M.V., and Miller, E.K. (2012). The role of prefrontal dopamine D1 receptors in the neural mechanisms of associative learning. Neuron *74*, 874–886. https://doi.org/10.1016/j.neuron.2012.04.018.
12. Surmeier, D.J., Obeso, J.A., and Halliday, G.M. (2017). Selective neuronal vulnerability in Parkinson disease. Nat. Rev. Neurosci. *18*, 101–113. https://doi.org/10.1038/nrn.2016.178.
13. Murphy, M.D., and Heller, E.A. (2022). Convergent actions of stress and stimulants via epigenetic regulation of neural circuitry. Trends Neurosci. *45*, 955–967. https://doi.org/10.1016/j.tins.2022.10.001.
14. Mi, W., Guan, H., Lyu, J., Zhao, D., Xi, Y., Jiang, S., Andrews, F.H., Wang, X., Gagea, M., Wen, H., et al. (2017). YEATS2 links histone acetylation to tumorigenesis of non-small cell lung cancer. Nat. Commun. *8*, 1088. https://doi.org/10.1038/s41467-017-01173-4.
15. Pant, D., Kakani, P., Joshi, R., Sabu, A., Agrawal, S., Samaiya, A., and Shukla, S. (2025). Interplay of YEATS2 and GCDH regulates histone crotonylation and drives EMT in head and neck cancer. eLife *14*, RP103321. https://doi.org/10.7554/eLife.103321.
16. Yeewa, R., Pohsa, S., Yamsri, T., Wongkummool, W., Jantaree, P., Potikanond, S., Nimlamool, W., Shotelersuk, V., Lo Piccolo, L., and Jantrapirom, S. (2024). The histone acylation reader ENL/AF9 regulates aging in Drosophila melanogaster. Neurobiol. Aging *144*, 153–162. https://doi.org/10.1016/j.neurobiolaging.2024.10.002.
17. Zhang, J., Gundu, A., and Strahl, B.D. (2021). Recognition of acetylated histone by Yaf9 regulates metabolic cycling of transcription initiation and chromatin regulatory factors. Genes Dev. *35*, 1678–1692. https://doi.org/10.1101/gad.348904.121.
18. Hardie, R.C., Raghu, P., Moore, S., Juusola, M., Baines, R.A., and Sweeney, S.T. (2001). Calcium influx via TRP channels is required to maintain PIP2 levels in Drosophila photoreceptors. Neuron *30*, 149–159. https://doi.org/10.1016/s0896-6273(01)00269-0.
19. Pfeil, E.M., Brands, J., Merten, N., Vogtle, T., Vescovo, M., Rick, U., Albrecht, I.M., Heycke, N., Kawakami, K., Ono, Y., et al. (2020). Heterotrimeric G Protein Subunit Galphaq Is a Master Switch for Gbetagamma-Mediated Calcium Mobilization by Gi-Coupled GPCRs. Mol. Cell *80*, 940–954.e946. https://doi.org/10.1016/j.molcel.2020.10.027.
20. Yau, K.W., and Hardie, R.C. (2009). Phototransduction motifs and variations. Cell *139*, 246–264. https://doi.org/10.1016/j.cell.2009.09.029.
21. Agam, K., von Campenhausen, M., Levy, S., Ben-Ami, H.C., Cook, B., Kirschfeld, K., and Minke, B. (2000). Metabolic stress reversibly activates the Drosophila light-sensitive channels TRP and TRPL in vivo. J. Neurosci. *20*, 5748–5755. https://doi.org/10.1523/JNEUROSCI.20-15-05748.2000.
22. Brands, J., Bravo, S., Jürgenliemke, L., Grätz, L., Schihada, H., Frechen, F., Alenfelder, J., Pfeil, C., Ohse, P.G., Hiratsuka, S., et al. (2024). A molecular mechanism to diversify Ca(2+) signaling downstream of Gs protein-coupled receptors. Nat. Commun. *15*, 7684. https://doi.org/10.1038/s41467-024-51991-6.
23. Zhang, Y., Rózsa, M., Liang, Y., Bushey, D., Wei, Z., Zheng, J., Reep, D., Broussard, G.J., Tsang, A., Tsegaye, G., et al. (2023). Fast and sensitive GCaMP calcium indicators for imaging neural populations. Nature *615*, 884–891. https://doi.org/10.1038/s41586-023-05828-9.
24. Chakraborty, P., Deb, B.K., Arige, V., Musthafa, T., Malik, S., Yule, D.I., Taylor, C.W., and Hasan, G. (2023). Regulation of store-operated Ca(2+) entry by IP(3) receptors independent of their ability to release Ca(2). eLife *12*, e80447. https://doi.org/10.7554/eLife.80447.
25. Feske, S., Gwack, Y., Prakriya, M., Srikanth, S., Puppel, S.H., Tanasa, B., Hogan, P.G., Lewis, R.S., Daly, M., and Rao, A. (2006). A mutation in Orai1

causes immune deficiency by abrogating CRAC channel function. Nature *441*, 179–185. https://doi.org/10.1038/nature04702.

26. Yeromin, A.V., Zhang, S.L., Jiang, W., Yu, Y., Safrina, O., and Cahalan, M.D. (2006). Molecular identification of the CRAC channel by altered ion selectivity in a mutant of Orai. Nature *443*, 226–229. https://doi.org/10.1038/nature05108.
27. Ohga, K., Takezawa, R., Arakida, Y., Shimizu, Y., and Ishikawa, J. (2008). Characterization of YM-58483/BTP2, a novel store-operated Ca2+ entry blocker, on T cell-mediated immune responses in vivo. Int. Immunopharmacol. *8*, 1787–1792. https://doi.org/10.1016/j.intimp.2008.08.016.
28. Pathak, T., Agrawal, T., Richhariya, S., Sadaf, S., and Hasan, G. (2015). Store-Operated Calcium Entry through Orai Is Required for Transcriptional Maturation of the Flight Circuit in Drosophila. J. Neurosci. *35*, 13784–13799. https://doi.org/10.1523/JNEUROSCI.1680-15.2015.
29. Hendrich, J., Van Minh, A.T., Heblich, F., Nieto-Rostro, M., Watschinger, K., Striessnig, J., Wratten, J., Davies, A., and Dolphin, A.C. (2008). Pharmacological disruption of calcium channel trafficking by the alpha2delta ligand gabapentin. Proc. Natl. Acad. Sci. USA *105*, 3628–3633. https://doi.org/10.1073/pnas.0708930105.
30. Khuong, T.M., Hamoudi, Z., Manion, J., Loo, L., Muralidharan, A., and Neely, G.G. (2019). Peripheral straightjacket (alpha2delta Ca(2+) channel subunit) expression is required for neuropathic sensitization in Drosophila. Philos. Trans. R. Soc. Lond. B Biol. Sci. *374*, 20190287. https://doi.org/10.1098/rstb.2019.0287.
31. Abu-Omar, N., Das, J., Szeto, V., and Feng, Z.P. (2018). Neuronal Ryanodine Receptors in Development and Aging. Mol. Neurobiol. *55*, 1183–1192. https://doi.org/10.1007/s12035-016-0375-4.
32. Zhao, F., Li, P., Chen, S.R., Louis, C.F., and Fruen, B.R. (2001). Dantrolene inhibition of ryanodine receptor Ca2+ release channels. Molecular mechanism and isoform selectivity. J. Biol. Chem. *276*, 13810–13816. https://doi.org/10.1074/jbc.M006104200.
33. Surmeier, D.J., Guzman, J.N., Sanchez-Padilla, J., and Schumacker, P.T. (2011). The role of calcium and mitochondrial oxidant stress in the loss of substantia nigra pars compacta dopaminergic neurons in Parkinson's disease. Neuroscience *198*, 221–231. https://doi.org/10.1016/j.neuroscience.2011.08.045.
34. Bozzi, Y., and Borrelli, E. (2013). The role of dopamine signaling in epileptogenesis. Front. Cell. Neurosci. *7*, 157. https://doi.org/10.3389/fncel.2013.00157.
35. Quintela-López, T., Shiina, H., and Attwell, D. (2022). Neuronal energy use and brain evolution. Curr. Biol. *32*, R650–R655. https://doi.org/10.1016/j.cub.2022.02.005.
36. Lee, K.S., Huh, S., Lee, S., Wu, Z., Kim, A.K., Kang, H.Y., and Lu, B. (2018). Altered ER-mitochondria contact impacts mitochondria calcium homeostasis and contributes to neurodegeneration in vivo in disease models. Proc. Natl. Acad. Sci. USA *115*, E8844–E8853. https://doi.org/10.1073/pnas.1721136115.
37. Amaral, A.U., and Wajner, M. (2020). Recent Advances in the Pathophysiology of Fatty Acid Oxidation Defects: Secondary Alterations of Bioenergetics and Mitochondrial Calcium Homeostasis Caused by the Accumulating Fatty Acids. Front. Genet. *11*, 598976. https://doi.org/10.3389/fgene.2020.598976.
38. Ewels, P.A., Peltzer, A., Fillinger, S., Patel, H., Alneberg, J., Wilm, A., Garcia, M.U., Di Tommaso, P., and Nahnsen, S. (2020). The nf-core framework for community-curated bioinformatics pipelines. Nat. Biotechnol. *38*, 276–278. https://doi.org/10.1038/s41587-020-0439-x.
39. Di Tommaso, P., Chatzou, M., Floden, E.W., Barja, P.P., Palumbo, E., and Notredame, C. (2017). Nextflow enables reproducible computational workflows. Nat. Biotechnol. *35*, 316–319. https://doi.org/10.1038/nbt.3820.
40. Krueger, F. (2015). Trim Galore!: A wrapper around Cutadapt and FastQC to consistently apply adapter and quality trimming to FastQ files, with extra functionality for RRBS data. https://github.com/FelixKrueger/TrimGalore.
41. Bushnell, B. (2014). BBMap: A Fast, Accurate, Splice-Aware Aligner (Lawrence Berkeley National Laboratory. *LBNL-7065E*).
42. Kopylova, E., Noé, L., and Touzet, H. (2012). SortMeRNA: fast and accurate filtering of ribosomal RNAs in metatranscriptomic data. Bioinformatics *28*, 3211–3217. https://doi.org/10.1093/bioinformatics/bts611.
43. Hoskins, R.A., Carlson, J.W., Wan, K.H., Park, S., Mendez, I., Galle, S.E., Booth, B.W., Pfeiffer, B.D., George, R.A., Svirskas, R., et al. (2015). The Release 6 reference sequence of the Drosophila melanogaster genome. Genome Res. *25*, 445–458. https://doi.org/10.1101/gr.185579.114.
44. Kim, D., Paggi, J.M., Park, C., Bennett, C., and Salzberg, S.L. (2019). Graph-based genome alignment and genotyping with HISAT2 and HISAT-genotype. Nat. Biotechnol. *37*, 907–915. https://doi.org/10.1038/s41587-019-0201-4.
45. Li, H., Handsaker, B., Wysoker, A., Fennell, T., Ruan, J., Homer, N., Marth, G., Abecasis, G., and Durbin, R.; 1000 Genome Project Data Processing Subgroup (2009). The Sequence Alignment/Map format and SAMtools. Bioinformatics *25*, 2078–2079. https://doi.org/10.1093/bioinformatics/btp352.
46. Smith, T., Heger, A., and Sudbery, I. (2017). UMI-tools: modeling sequencing errors in Unique Molecular Identifiers to improve quantification accuracy. Genome Res. *27*, 491–499. https://doi.org/10.1101/gr.209601.116.
47. Kovaka, S., Zimin, A.V., Pertea, G.M., Razaghi, R., Salzberg, S.L., and Pertea, M. (2019). Transcriptome assembly from long-read RNA-seq alignments with StringTie2. Genome Biol. *20*, 278. https://doi.org/10.1186/s13059-019-1910-1.
48. Love, M.I., Huber, W., and Anders, S. (2014). Moderated estimation of fold change and dispersion for RNA-seq data with DESeq2. Genome Biol. *15*, 550. https://doi.org/10.1186/s13059-014-0550-8.
49. Cheng, J., Hsu, L.F., Juan, Y.H., Liu, H.P., and Lin, W.Y. (2021). Pathway-targeting gene matrix for Drosophila gene set enrichment analysis. PLoS One *16*, e0259201. https://doi.org/10.1371/journal.pone.0259201.
50. Song, W., Podicheti, R., Rusch, D.B., and Tracey, W.D. (2023). Transcriptome-wide analysis of pseudouridylation in Drosophila melanogaster. G3 (Bethesda) *13*, jkac333. https://doi.org/10.1093/g3journal/jkac333.
51. Jantrapirom, S., Lo Piccolo, L., Yoshida, H., and Yamaguchi, M. (2018). A new Drosophila model of Ubiquilin knockdown shows the effect of impaired proteostasis on locomotive and learning abilities. Exp. Cell Res. *362*, 461–471. https://doi.org/10.1016/j.yexcr.2017.12.010.

STAR★METHODS

KEY RESOURCES TABLE

REAGENT or RESOURCE	SOURCE	IDENTIFIER
Antibodies		
Actin	Developmental Studies Hybridoma Bank	JLA20; RRID: AB_528068
Fasciclin-2 (FasII)	Developmental Studies Hybridoma Bank	1D4; RRID: AB_528235
GFP	Invitrogen	A-11122; RRID: AB_221569
Tyrosine hydroxylase (TH)	Merck	AB152; RRID: AB_390204
Anti-mouse IgG (H + L)-HRP Conjugate	Biorad	Cat#1706516; RRID: AB_2921252
Anti-rabbit IgG (H + L)-HRP Conjugate	Biorad	Cat#1706515; RRID: AB_11125142
Goat anti-rabbit IgG conjugated with Alexa Fluor® 594	Invitrogen	A-11012; RRID: AB_2534079
Goat anti-mouse IgG conjugated with Alexa Fluor® 594	Invitrogen	A-11032: RRID: AB_2534073
Chemicals, peptides, and recombinant proteins		
BTP2 (also known as YM-58483)	Med Chem Express (MCE)	HY-100831
Gabapentin	TargetMol	T0702
Dantrolene	Med Chem Express (MCE)	HY-12542
Schneider's Drosophila Medium	PAN-Biotech GmbH	P04-91500
Vectashield Vibrance antifade mounting medium	VectorLabs	H-1700
Protease Inhibitor Cocktail	HIMEDIA	ML051
Deposited data		
Raw and DESeq2-normalized RNA-seq data	Gene Expression Omnibus	GSE:GSE307078
Experimental models: Organisms/strains		
nSyb-Gal4	Bloomington *Drosophila* Stock Center	68222
Ddc-GAL4	Bloomington *Drosophila* Stock Center	7009
elav-GAL4	Bloomington *Drosophila* Stock Center	8760
OK371-GAL4	Bloomington *Drosophila* Stock Center	26160
OK107-GAL4	Bloomington *Drosophila* Stock Center	854
UAS-mCherry RNAi	Bloomington *Drosophila* Stock Center	35785
UAS-Luc RNAi	Bloomington *Drosophila* Stock Center	31603
UAS-dYEATS2 RNAi	Vienna *Drosophila* Resource Center	105606
UAS-dENL/AF9 RNAi	Bloomington *Drosophila* Stock Center	34798
UAS-mCD8-EGFP	Bloomington *Drosophila* Stock Center	5137
UAS-Orai^{E180A}	Bloomington *Drosophila* Stock Center	602870
UAS-GCAMP6s	Bloomington *Drosophila* Stock Center	42746
UAS-trp IR	Bloomington *Drosophila* Stock Center	61352
UAS-mCD8-EGFP;UAS-NTC IR	This study	N/A
UAS-mCD8-EGFP;UAS-dYEATS2 IR	This study	N/A
UAS-Orai^{E180A};UAS-dYEATS2 IR	This study	N/A
UAS-trp IR; UAS-dYEATS2 IR	This study	N/A
Oligonucleotide primers	MACROGEN	see Table S3
Software and algorithms		
CellSense Dimsnion software v3.2	Olympus	N/A
GSEA software v4.3.2	Broad Institute	RRID:SCR_003199
GraphPad software v.9	GraphPad Software	RRID:SCR_002798
R softaware v4.1	R Foundation for Statistical Computing	RRID:SCR_001905
Other		
RNA-seq data (raw and DESeq2-normalized)	This study	GEO:GSE307078

EXPERIMENTAL MODEL AND STUDY PARTICIPANT DETAILS

Drosophila husbandry

Drosophila melanogaster stocks were maintained on standard cornmeal–yeast–glucose medium at 22 °C with 60% humidity under a 12:12 light/dark cycle, unless otherwise specified. The GAL4/UAS binary system[22] was employed for tissue-specific knockdown or overexpression. Pan-neuronal manipulations were driven by nSyb-GAL4, while dopaminergic, glutamatergic, or mushroom body–specific expression was achieved using Ddc-GAL4, OK371-GAL4, and OK107-GAL4 drivers, respectively, at 25 °C. The full list of strains used in this study is provided in Table S2 and key resources table. To minimize genetic background effects, all experimental flies were backcrossed six times with the *w* strain before use. Unless otherwise indicated, experiments were performed on adult male flies within 5 days post-eclosion. Sensitivity to electric stimulation was assessed in wandering third-instar larvae of both sexes. All Drosophila experiments were approved by the Institutional Animal Care and Use Committee of the Faculty of Medicine, Chiang Mai University, Thailand (IRB#18/2565).

METHOD DETAILS

Library preparation and RNA sequencing (RNA-seq)

For transcriptomic analysis, 3-day-old male flies of each genotype were collected, snap-frozen in liquid nitrogen, and decapitated. Total RNA was extracted from 50 heads per replicate (three biological replicates per group) using the RNeasy Mini Kit (Qiagen, Valencia, CA) following the manufacturer's instructions. The RNA samples, stabilized under ethanol precipitation conditions, were submitted to Macrogen, Inc. (Korea) for RNA sequencing (RNA-Seq). Prior to sequencing, the samples were analyzed with an Agilent 2100 Bioanalyzer to assess overall quality. Only samples with an RNA Integrity Number (RIN) > 7 and an rRNA ratio >1 were processed further. RNA-sequencing libraries were prepared using the TruSeq Stranded mRNA Library Prep Kit, and sequencing was performed on the Illumina NovaSeq 6000 platform with a read length of 100 bp paired-end, generating approximately 30 million reads per sample.

Quality control and preprocessing of RNA-seq data

Illumina short-read sequencing data were retrieved from Macrogen's online repository and then transferred to the local server – MedCMU HPC – for analysis. Raw FASTQ files were processed using the nf-core/rnaseq pipeline v3.14.0[38] executed via Nextflow environments.[39] Specifically, per-sample quality control was performed with FastQC v0.12.0; adapter trimming was conducted with Trim Galore! v0.6.5[40]; putative genome contaminants were removed using BBSplit[41]; and rRNA was depleted *in silico* with SortMeRNA.[42] Clean reads were aligned to the *Drosophila melanogaster* reference genome BDGP6 (dm6)[43] using HiSat2.[44] The resulting BAM files were coordinate-sorted and indexed using SAMtools.[45] Duplicate molecules in UMI-tagged libraries were collapsed with UMI-tools,[46] while duplicates in non-UMI libraries were marked with Picard MarkDuplicates. Summary metrics of all replicates from different tools were compiled with MultiQC V1.19 (Table S1). Reference-guided quantification was performed with StringTie2[47] against the Ensembl release 81. Count data generated by StringTie2 in quantification-only mode were then used as input for differential expression analysis with the DESeq2 package[48] in the R software environment v4.1.

Functional enrichment analysis

The matrix of DESeq2 normalized read counts (median of ratios) was used as an input of expression dataset for Gene Set Enrichment Analysis (GSEA) analysis, which was performed with GSEA software version 4.3.2 on predefined gene sets derived from 137 KEGG pathways in *D. melanogaster*.[49] To identify concordantly regulated pathways between the knockdown and control groups, GSEA was conducted using the following parameters: permute = gene set, metric = Signal2Noise, and scoring_scheme = weighted,[50] with the Kolmogorov-Smirnov statistic. Gene sets with a false discovery rate (FDR) < 0.05 were considered significantly deregulated and enriched gene sets. Leading-edge analysis was then performed on the considerably enriched gene sets in GSEA. A Heatmap of candidate gene lists and a bubble plot based on the GSEA analysis were plotted by an online platform for data analysis and visualization (http://www.bioinformatics.com.cn/srplot).

RNA extraction and RT-qPCR

Total RNA was extracted from *Drosophila* tissues using the RNeasy Mini Kit (QIAGEN) according to the manufacturer's instructions. Three independent biological replicates were prepared. RNA quality and concentration were measured with a NanoDrop One/OneC spectrophotometer (Thermo Fisher Scientific). For cDNA synthesis, 1 μg of RNA was reverse transcribed using the SensiFAST cDNA Synthesis Kit (Bioline). Quantitative RT-PCR (RT-qPCR) was performed in technical triplicates for each biological replicate with the SensiFAST SYBR Lo-ROX Kit on a CFX Opus Real-Time PCR System (Bio-Rad), employing gene-specific primers (Table S3). *ACT5C* was used as a reference gene for normalization.

Protein extraction and western blotting

Protein extracts were obtained from adult *Drosophila* heads using RIPA Lysis and Extraction Buffer (Thermo Fisher) supplemented with protease inhibitors. Approximately 40 heads were homogenized in 100 μL of buffer, followed by incubation at 4 °C with gentle

agitation for 20 min. Lysates were cleared by centrifugation at 14,000 × g for 20 min at 4 °C, and protein concentrations were determined using the BCA Protein Assay Kit (Millipore #71285). Equal amounts of protein (30 μg) were separated on 12% polyacrylamide gels and transferred to Immobilon-P PVDF membranes (Merck) with the Trans-Blot Turbo transfer system (Bio-Rad). Membranes were blocked in 5% skim milk prepared in TBS-T (Tris-buffered saline, 0.1% Tween 20) and incubated overnight at 4 °C with the indicated primary antibodies (Table S4). After four washes with TBS-T, membranes were exposed to HRP-conjugated secondary antibodies (1:3000) for 1 hour at room temperature. Both primary and secondary antibodies were diluted in 5% skim milk/TBS-T. Signals were visualized using WesternSure chemiluminescent reagents (LI-COR) and captured with a C-DiGit Blot Scanner (LI-COR). Protein expression was normalized to Actin, and band intensities were quantified with ImageJ (v1.53k) across independent biological replicates. Additional information on chemicals is listed in Table S5.

Brain dissection and imaging

Brains from 5-day-old adult flies carrying the pan-neuronal driver and UAS-GCaMP6s were dissected in ice-cold 1× PBS. Following dissection, tissues were incubated *ex vivo* for 20 min at 25 °C in PBS supplemented with either 200 mM NaCl, 200 mM KCl, or 200 mM glucose. After incubation, brains were mounted on glass slides using antifade mounting medium and imaged for GFP fluorescence. For analysis of specific neuronal populations and mushroom body architecture, brains from 5-day-old adults were dissected in Schneider's *Drosophila* medium and fixed in 4% formaldehyde prepared in PBS for 30 min. Samples were then rinsed three times for 20 min each in PBS containing 0.3% Triton X-100, followed by blocking in PBS with 0.3% Triton X-100 and 0.2% bovine serum albumin for 30 min. Primary antibodies, mouse anti-FasII (1D4, Developmental Studies Hybridoma Bank) or rabbit anti-TH (AB152, Merck), were applied in blocking buffer and incubated for 48h at 4 °C. Brains were subsequently washed and incubated overnight at 4°C with Alexa Fluor-conjugated secondary antibodies (Table S4). Images were acquired using an Olympus Fluoview FV3000 confocal microscope equipped with a Plan Apo 20×/0.80 objective lens. Identical laser and detector settings were used across experimental groups to ensure comparability. Z-stacks were collected at 2048 × 2048-pixel resolution, with 12 optical sections (4 μm step size), and processed as maximum-intensity projections oriented from posterior to anterior.

Quantification of dopaminergic neuronal clusters and colocalization analysis

To measure the extent of GFP-labelled neuronal populations, flies expressing UAS-mCD8-GFP under the control of specific neuronal drivers were analyzed. Maximum projection images were generated from confocal stacks using CellSense Dimension software (version 3.2, Olympus). Threshold levels for object detection were established using control samples (*mCD8-GFP; NTC-IR*), and the same parameters were subsequently applied to experimental genotypes (*mCD8-GFP; dYEATS2-IR*). Quantification was performed within defined regions of interest (ROIs), and automated object detection and measurement were used to calculate the total number of GFP-positive neurons per ROI. To assess the subset of DAergic neurons with functional activity, we quantified colocalization between GFP and TH immunoreactivity. In this context, GFP marked neurons expressing UAS-mCD8-GFP under control of the Ddc-GAL4 driver, while TH served as a definitive marker of dopamine-producing neurons. Confocal z-stacks were imported into CellSense Dimension software (version 3.2, Olympus), and colocalization analyses of GFP and TH channels were performed across 12 optical sections (4 μm each). ROIs were drawn around the central brain lobes. Scatterplots of the two channels were generated, and colocalization files were created for each ROI. Segmentation was applied with a minimum object size of 50 pixels, followed by automatic thresholding to standardize detection. Quantification of GFP-positive, TH-positive, and colocalized (GFP^+/TH^+) neurons was then performed to determine the proportion of functionally dopaminergic cells.

Seizure-like behaviors

Mechanical stress–induced seizure susceptibility was assessed using the bang-sensitivity assay, adapted from previously described protocols.[9] Newly eclosed males were aged for 3–4 days and gently transferred individually into empty vials using a suction pipette to avoid CO_2 anesthesia. After a 5-min acclimation period, flies were subjected to a 10-s high-speed vortex. Immediately thereafter, they were placed in a 15-cm glass Petri dish and video-recorded for offline analysis. Seizure-like behavior (SLB) was defined as uncontrolled movements or paralysis persisting for more than 3 s after mechanical stimulation. Recovery time was recorded, and values were compared with genotype-matched controls. For each genotype, a minimum of 50 flies was analyzed.

Electric shock-induced seizure susceptibility in larvae was assessed using a grid-based stimulation assay (*Drosophila* Larval Electric Stimulator, DL-ES), as previously described.[9] Briefly, foraging third-instar larvae were placed on an 8 × 5 cm electrified grid connected to an Arduino Uno microcontroller board delivering a square pulse output of 7 V direct current (DC). Larvae were allowed to acclimate to the testing environment prior to stimulation. A single 2-s electric pulse was then applied, inducing sustained contractions of the body wall muscles and occasional spasms that interrupted normal crawling behavior. The time from stimulus onset to the resumption of coordinated crawling was measured and compared with control groups. A total of 100 larvae were analyzed per genotype or experimental condition.

All behavioral experiments were conducted under standardized illumination provided by a 5600 K LED light source and performed at the same time of day to minimize variability related to circadian rhythms. Assays were carried out within a 3–4 h afternoon window (zeitgeber time ZT5–ZT9). All experimental procedures and data analyses were performed with the experimenter blinded to genotype and treatment conditions.

Climbing assay

Adult locomotor performance was evaluated using a climbing paradigm adapted from.[51] Male flies of each genotype were collected at eclosion and aged for 3, 9, 15, 21, or 27 days. Groups of ten age-matched flies were transferred, without anesthesia, into clear conical tubes and allowed to acclimate for 10 min. To initiate climbing, tubes were gently tapped to displace the flies to the bottom; this stimulus was applied at 30-s intervals and repeated five times for each group. Climbing behavior was video recorded, and performance was quantified by scoring the vertical distance reached within 5 s: 0 (<2.0 cm), 1 (2.0–3.9 cm), 2 (4.0–5.9 cm), 3 (6.0–7.9 cm), 4 (8.0–9.9 cm), and 5 (≥10.0 cm). A climbing index was calculated for each group by multiplying the number of flies in each category by its score, summing across categories, and dividing by the total number of flies. For each genotype, assays were performed on at least 100 flies, and values were compared with genotype-matched controls. Experimental execution and data analysis were carried out under blinded conditions with respect to genotype and treatment.

QUANTIFICATION AND STATISTICAL ANALYSIS

All statistical analyses were performed using GraphPad Prism 9 (GraphPad Software). For datasets following a normal distribution, two-group comparisons were assessed with either Student's *t* test or Welch's *t* test, while differences among more than two groups were evaluated using one-way ANOVA with followed by the appropriate post-hoc test as indicated for each experiment. When data did not meet normality assumptions, the Mann-Whitney U test was applied for pairwise comparisons, and the Kruskal–Walli's test with Dunn's post hoc analysis was used for multiple groups. A p-value <0.05 was considered statistically significant. Results are shown as mean ± standard deviation (SD) for experiments with fewer than six replicates (e.g., Western blotting and qPCR), and as mean ± standard error of the mean (SEM) for larger datasets such as behavioral assays. Statistical significance is denoted by asterisks as follows: $^{*}p < 0.05$, $^{**}p < 0.01$, $^{***}p < 0.001$, $^{****}p < 0.0001$; ns, not significant.